A new method for accurate retrieval of atomic dipole phase or photoionization group delay in attosecond photoelectron streaking experiments

IOP Publishing Journal of Optics
J. Opt. 19 (2017) 114009 (9pp) https://doi.org/10.1088/2040-8986/aa8fb6

A new method for accurate retrieval of atomic dipole phase or photoionization group delay in attosecond photoelectron streaking experiments

Xi Zhao[1], Hui Wei[1], Changli Wei[2] and C D Lin[1]

[1] Department of Physics, Kansas State University, Manhattan, KS 66506, United States of America
[2] School of Physics and Electronics, Qiannan Normal College For Nationalities, Duyun, Guizhou 558000, People's Republic of China

E-mail: zhaoxi719@phys.ksu.edu

Received 23 June 2017, revised 25 September 2017
Accepted for publication 28 September 2017
Published 20 October 2017

Abstract

In recent years, attosecond streaking experiments have been used to extract the phase of photoionization dipole transition matrix element (or the photoionization group delay) in atoms, molecules and condensed materials. The most accurate retrieval method so far is based on the frequency-resolved optical gating for complete reconstruction of attosecond bursts (FROG-CRAB). However, the FROG-CRAB employs a number of approximations that would cause errors in the retrieved results. In this article, we applied our recently proposed attosecond pulse characterization method phase retrieval of broadband pulses (PROBP) to the retrieval of photoionization group delay difference between Ne($2p$) and Ne($2s$) ionization channels, and between Ar($3p$) and Ne($2p$) channels. Our simulations demonstrate that more accurate results can be retrieved using PROBP than using FROG-CRAB, and cast doubts on group delays reported in previous streaking measurements.

Keywords: attosecond streaking, delay in photoionization, FROG-CRAB, PROBP

(Some figures may appear in colour only in the online journal)

1. Introduction

With the advent of attosecond pulse trains (APT) and isolated attosecond pulses (IAP) [1–13] since 2001, attosecond pulses have been used to initiate photoionization of atoms [14–29], molecules [30–34] and condensed materials [35–40]. The goal is that the attosecond electron wave packets generated can then be probed by another attosecond pulse with different time delays, therefore electron dynamics can be probed at attosecond timescale. This has not been possible so far, thus the 'probe' usually is a moderate intense infrared (IR) laser. By measuring the continuum photoelectron spectra versus the time delay between the extreme ultraviolet (XUV) attosecond pulse and the IR pulse, the two-dimensional photoelectron spectrogram can be obtained. Such an experimental setup is called attosecond streaking [41]. In fact, the streaking spectrogram is widely used to characterize attosecond pulses, by employing the 'reconstruction of attosecond beating by interference of two-photon transition' [42] method for the characterization of APTs, and the 'frequency-resolved optical gating for complete reconstruction of attosecond bursts' (FROG-CRAB) method [43] for the characterization of IAPs. In this article, we focus on attosecond streaking using IAPs. The FROG-CRAB method assumes that one can extract a photoelectron wave packet from the spectrogram by using this method. The wave packet consists of the XUV field and the complex photoionization transition dipole moment of the target. To characterize the IAP, one has to know the transition dipole. If the target is a rare gas atom, then the magnitude of the transition dipole as a function of the photoelectron energy is well known from synchrotron radiation measurement, however the phase of the transition dipole has to rely on

theoretical calculations. On the other hand, if the fields of the attosecond pulse and the IR are known well, from the retrieved wave packet one would hope that the phase of the transition dipole can be obtained.

In the past decade, instead of retrieving the phase of the transition dipole from the experimental streaking spectra, the derivative of the phase with respect to the photoelectron energy, which was referred to as the 'photoionization time delay', was generally reported. This concept was an extension of the Eisenbud–Wigner–Smith delay [44–46] in scattering process. As we know in optics, the derivative of the spectral phase has been *defined* as the group delay. Similarly, the photoionization time delay used here is the energy derivative of the phase of the photoionization dipole moment so that it should be called a 'Wigner group delay'. This interpretation is still a matter of ongoing research and the concept of photoionization time delay is not fully clear yet [47, 48]. In addition, the phase of a photoelectron wave packet should be specified across the whole spectral bandwidth. In terms of group delay, it should also be specified over the whole bandwidth. The two quantities amount to the same thing except for a trivial constant phase. On the other hand, specifying the group delay or the phase at the peak energy of the photoelectron spectrum does not specify the wave packet. Thus, the goal of the streaking experiment is either to retrieve the phase or the group delay over the whole spectral bandwidth. This can be done by using FROG-CRAB but not by the center-of-mass method that has been widely used in the literature [35, 36, 53, 54].

In a typical streaking experiment, the XUV phase is unknown, thus experiments are carried out by a single XUV pulse to initiate photoionization through two separate ionization channels which can be in the same target or in different targets. From the two streaking spectrograms, one may extract two electron wave packets. The dipole phase difference between the two channels is expected to be the phase difference of the two electron wave packets, whereas the unknown XUV phase is assumed to be canceled after taking difference. FROG-CRAB has been employed to extract the Wigner group delay between the $2p$ and $2s$ channels of Ne [22], and between Ar($3p$) and Ne($2p$) channels [23]. We mentioned that both experiments reported the time delay difference but to avoid confusion we believe that they should be called the group delay difference. In [22], the group delay difference at the peak photon energy of the XUV pulse was reported, while in [23] the group delay difference over the spectral region of the XUV was reported. In the meanwhile, a lot of theoretical works have been invoked to interpret these reported group delays retrieved from FROG-CRAB [48–58]. Although up to now there has been no theory that could completely explain the experimental measured group delay, theorists are making progress on understanding the streaking experiment. The interaction between the photoelectron and its parent ion in the laser field (so-called Coulomb-laser coupling) is believed to be a critical effect that has not been included in the FROG-CRAB method. On the other hand, the possible errors on the group delays extracted from the streaking spectra have not been addressed for a long time.

The FROG-CRAB method relies on the strong field approximation (SFA), wave packet approximation (WPA) as well as the central momentum approximation (CMA). It has been demonstrated that the CMA is detrimental to the dipole phase retrieval, especially when the XUV pulse has large attochirp [59, 60]. Recently, we proposed a B-Spline function based fitting algorithm—'phase retrieval of broadband pulses' (PROBP), which was used to retrieve the XUV phase and IR field [61]. In this article, our aim is to demonstrate that PROBP can also be used to extract the dipole phase or Wigner group delay, and is more accurate than FROG-CRAB since the PROBP method has removed the additional CMA imposed by the FROG-CRAB. Our simulations are based on SFA, where the interactions between the photoelectron and the ionic core are neglected, which is valid for high-energy photoelectrons. Within the SFA model, the result obtained from the streaking spectrogram can be directly compared with the input Wigner group delay. In the following sections, we will use 'photoionization group delay' and 'Wigner group delay' interchangeably.

The article is organized as the following: section 2 briefly introduces the principle of PROBP; in section 3, we run various simulations using different targets and XUV pulses, and compare the retrieved photoionization group delays from PROBP with those from FROG-CRAB; section 3.1 shows the result for photoionization from $2p$ and $2s$ states of Ne, and section 3.2 shows the result for photoionization from Ar($3p$) and Ne($2p$); section 4 discusses the effect of WPA and CMA; section 5 gives the conclusion. Atomic units are used unless otherwise stated.

2. The principle of PROBP

Both the FROG-CRAB and PROBP methods assume that the measured photoelectron spectrogram can be modeled by SFA [43, 62]:

$$S(E, t_d) = \left| \int_{-\infty}^{\infty} E_{\mathrm{XUV}}(t - t_d) d\left(\frac{[p + A(t)]^2}{2}\right) \times \mathrm{e}^{-\mathrm{i}\varphi(p,t)} \mathrm{e}^{\mathrm{i}(E+I_P)t} \mathrm{d}t \right|^2. \quad (1)$$

Here, the polarization of the XUV, the IR, and the photoelectrons are all taken along the $+z$ direction. p is the asymptotic momentum of the photoelectron, and $E = p^2/2$ is its energy. $E_{\mathrm{XUV}}(t)$ is the XUV field in the time domain. In the frequency domain

$$\tilde{E}_{\mathrm{XUV}}(\Omega) = U(\Omega)\mathrm{e}^{\mathrm{i}\Phi(\Omega)} = \int_{-\infty}^{\infty} E_{\mathrm{XUV}}(t)\mathrm{e}^{\mathrm{i}\Omega t}\mathrm{d}t, \quad (2)$$

where $U(\Omega)$ and $\Phi(\Omega)$ are the XUV spectral amplitude and phase, respectively. In equation (1), $A(t) = -\int_{-\infty}^{t} E_{\mathrm{IR}}(t')\mathrm{d}t'$ is the vector potential of the IR field. The time delay between XUV and IR fields is denoted by t_d. A positive t_d means the XUV comes after the peak of the IR field. I_p is the ionization potential energy of the target. The phase function $\varphi(p, t)$

reads

$$\varphi(p, t) = \int_t^\infty \left[pA(t') + \frac{1}{2}A^2(t')\right]\mathrm{d}t'. \quad (3)$$

Equation (1) includes the single-photon transition dipole matrix element $\mathrm{d}(E) = \langle E\hat{z}|z|i\rangle$, where $|i\rangle$ is the initial bound state, and $|E\hat{z}\rangle$ is the continuum state in which the electron has an asymptotic momentum $p = \sqrt{2E}$ toward the $+z$ direction. The bound and continuum states are eigenstates of the field-free Hamiltonian of the target atom. The transition dipole is a complex quantity $\mathrm{d}(E) = |\mathrm{d}(E)|\mathrm{e}^{\mathrm{i}\eta(E)}$ which can be calculated within the single-active-electron approximation. The details of evaluating the transition dipole can be found in [59]. The Wigner group delay is then defined as

$$\tau(E) = \frac{\mathrm{d}}{\mathrm{d}E}\eta(E). \quad (4)$$

Without the IR field, the XUV pulse creates an photoelectron wave packet

$$\tilde{\chi}(E) = \tilde{E}_{\mathrm{XUV}}(\Omega)\mathrm{d}(E), \quad (5)$$

in which $\Omega = E + I_p$ is the energy of XUV photon. Equation (5) is derived from the first-order perturbation theory, which requires the XUV pulse to be weak (typically 10^{11} W cm^{-2} in peak intensity). The measured XUV-only photoelectron spectrum is proportional to $|\tilde{\chi}(E)|^2$, but the phase of the wave packet cannot be measured directly. By introducing the wave packet, the SFA model can be further replaced by the WPA:

$$S(E, t_d) = \left|\int_{-\infty}^{\infty} \chi(t - t_d)\mathrm{e}^{-\mathrm{i}\varphi(p,t)}\mathrm{e}^{\mathrm{i}(E+I_P)t}\mathrm{d}t\right|^2, \quad (6)$$

where $\chi(t)$ is the wave packet in the time domain

$$\chi(t) = \frac{1}{2\pi}\int_0^\infty \tilde{\chi}(E)\mathrm{e}^{-\mathrm{i}Et}\mathrm{d}E. \quad (7)$$

Note that although equation (6) seems to be separating the XUV ionization and the IR streaking processes, it is only an approximation to the SFA model equation (1) rather than an exact theory. The derivation of WPA was given in [63] where $E_{\mathrm{XUV}}(t)$ was expressed in terms of $\tilde{E}_{\mathrm{XUV}}(\Omega) = \frac{\tilde{\chi}(E)}{\mathrm{d}(E)}$ and $[\mathrm{d}(E)]^{-1}$ was expanded in a Taylor series, which eventually lead to equation (6). To get this result all derivatives of $A(t)$ should be neglected, which requires that the exponential factor $\mathrm{e}^{-\mathrm{i}\varphi(p,t)}$ oscillates as a function of t with a period much shorter than the optical cycle of the IR field [63].

If $S_1(E, t_d)$ and $S_2(E, t_d)$ are photoelectron spectrograms from two separate ionization channels under the same XUV and IR fields, FROG-CRAB and PROBP method may retrieve the two wave packets $\tilde{\chi}_1(E)$, $\tilde{\chi}_2(E)$ as well as the IR field $E_{\mathrm{IR}}(t)$. In order to cancel the XUV phase we have to compare the two wave packets at the same photon energy $\Omega = E + I_p$ instead of electron energy E. The dipole phase difference is obtained by

$$\eta_1(\Omega) - \eta_2(\Omega) = \arg\tilde{\chi}_1(\Omega) - \arg\tilde{\chi}_2(\Omega) \quad (8)$$

and then the difference in photoionization group delay between the two channels is given by

$$\Delta\tau_{1/2}(\Omega) = \frac{\mathrm{d}}{\mathrm{d}\Omega}[\eta_1(\Omega) - \eta_2(\Omega)]. \quad (9)$$

In the FROG-CRAB method, the phase function $\varphi(p, t)$ in equation (6) is replaced by $\varphi(p_0, t)$ with p_0 being the central momentum of the photoelectrons, which has been referred to as the CMA. Then several general projection algorithms [64, 65] can be applied to extract $\tilde{\chi}_1(E)$, $\tilde{\chi}_2(E)$ and $A(t)$. On the other hand, PROBP does not require CMA. In the PROBP method, the phase of the two wave packets are constructed by B-spline basis functions [66]:

$$\arg\tilde{\chi}_1(\Omega) = \sum_{i=1}^{n_1} a_i B_i^{k_1}(\Omega), \quad (10)$$

$$\arg\tilde{\chi}_2(\Omega) = \sum_{i=1}^{n_2} b_i B_i^{k_2}(\Omega). \quad (11)$$

The wave packet amplitude $|\tilde{\chi}_1(\Omega)|$ and $|\tilde{\chi}_2(\Omega)|$ are treated as known functions. The IR field is modeled in the time domain

$$E_{\mathrm{IR}}(t) = f(t)\cos(\omega_L t + \phi_{\mathrm{CEP}}). \quad (12)$$

We assume the central frequency ω_L and the carrier-envelope phase ϕ_{CEP} are known but the envelope $f(t)$ is not known, then $f(t)$ is expanded by B-spline basis functions as well:

$$f(t) = \sum_{i=1}^{n_3} c_i B_i^{k_3}(t). \quad (13)$$

Therefore, we have three sets of unknown parameters $\{a_i\}$, $\{b_i\}$ and $\{c_i\}$ which are the expansion coefficients of unknown functions $\arg\tilde{\chi}_1(\Omega)$, $\arg\tilde{\chi}_2(\Omega)$ and $f(t)$. B_i^k are B-spline basis functions of the kth order. n is the number of B-spline functions and i is the index. The expressions of B-spline basis functions have been given in our previous paper [61].

In PROBP, the optimal parameters $\{a_i, b_i, c_i\}$ are found by genetic algorithm (GA). From guessed parameters one can reconstruct $\arg\tilde{\chi}_1(\Omega)$, $\arg\tilde{\chi}_2(\Omega)$, $f(t)$ and then reconstruct two spectrograms $S_1^r(E, t_d)$ and $S_2^r(E, t_d)$ using equation (6) for the two ionization channels. Compared with the input spectrograms $S_1^i(E, t_d)$ and $S_2^i(E, t_d)$, the goal of the algorithm is to minimize the error function

$$E[a_i, b_i, c_i] = \sum_{k_1,l}[S_1^i(E_{k_1}, t_{d,l}) - S_1^r(E_{k_1}, t_{d,l})]^2 + \sum_{k_2,l}[S_2^i(E_{k_2}, t_{d,l}) - S_2^r(E_{k_2}, t_{d,l})]^2. \quad (14)$$

Here, we discretize $S_1(E, t_d)$ and $S_2(E, t_d)$ at two sets of points $\{E_{k_1}, t_{d,l}\}$ and $\{E_{k_2}, t_{d,l}\}$, respectively. Typically we chose 100–500 points in time delay and 100 points in energy. The GA runs a large number of generations (typically 50 000–100 000 generations) until convergence is achieved. The number and order of B-spline basis functions n_1, n_2, n_3 and k_1, k_2, k_3 are chosen in order to make the algorithm converge fast. More details about PROBP can be found in [61].

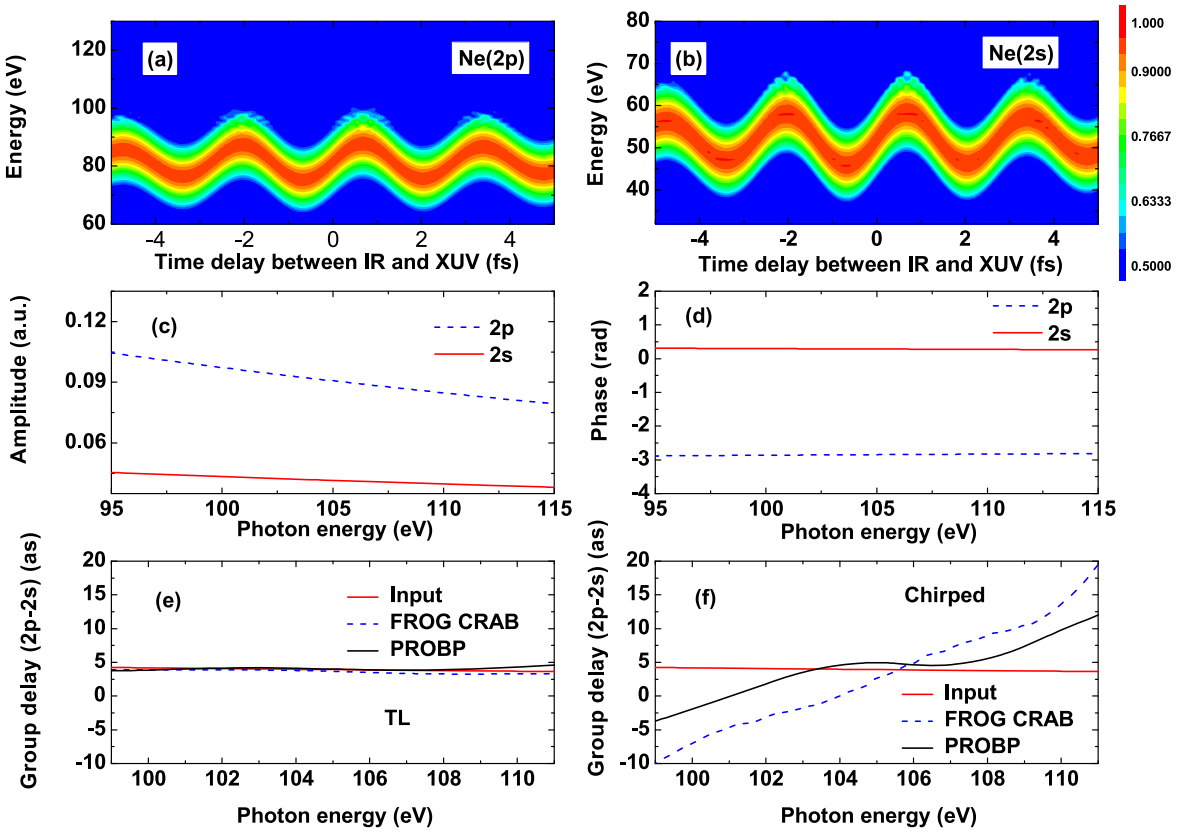

Figure 1. (a) Input Ne(2p) spectrogram using a 190 as TL XUV pulse. (b) Input Ne(2s) spectrogram using the same TL pulse. (c) Input dipole amplitude and (d) dipole phase for Ne 2p and 2s ionization channels. (e) Comparison between the input (red solid line) photoionization group delay (difference) $\Delta\tau_{2p/2s}$ and the retrieved group delay from PROBP (black solid line) and FROG-CRAB (blue dashed line) by using the 190 as TL XUV pulse. (f) Comparison between the input and retrieved group delay by using the 280 as chirped XUV pulse. Both XUV pulses are centered at $\Omega_0 = 105$ eV with a FWHM bandwidth $\Delta\Omega = 9$ eV. The IR field is 800 nm in wavelength, cosine-squared envelope, 6.2 fs in FWHM duration, and 10^{12} W cm^{-2} in peak intensity.

3. Photoionization group delays extracted by PROBP—compared with FROG-CRAB

3.1. Group delay between photoionization from 2p and 2s states of Ne

We first focus on the retrieval of photoionization group delay (difference) $\Delta\tau_{2p/2s}$ between 2p and 2s channels of Ne. Two XUV pulses are used in the simulation. One is transform-limited (TL) and the other is chirped. Both pulses have the same $U(\Omega)$ which takes a Gaussian form with a central photon energy $\Omega_0 = 105$ eV and a full width at half-maximum (FWHM) bandwidth $\Delta\Omega = 9$ eV. The TL pulse has a FWHM duration of 190 as and a peak intensity of 8×10^{11} W cm^{-2}. The chirped pulse has a quadratic phase $\Phi(\Omega) = \frac{1}{2}\mathrm{GDD}_X(\Omega - \Omega_0)^2$, with $\mathrm{GDD}_X = 0.0160$ fs^2 being the XUV group delay dispersion. Its FWHM duration increases to 280 as. The IR field is 800 nm in wavelength, cosine-squared envelope, 6.2 fs in FWHM duration, 10^{12} W cm^{-2} in peak intensity, and $\phi_{\mathrm{CEP}} = 0$. The input spectrograms are calculated using SFA equation (1). Figures 1(a) and (b) show the input spectrograms for 2p and 2s electrons using the TL XUV pulse, respectively. The dipole amplitude $|d(\Omega)|$ and phase $\eta(\Omega)$ for the two ionization channels are plotted in figures 1(c) and (d), respectively. The dipole phase of 2p and 2s channels vary smoothly in the photon energy range of the XUV pulse. The transition dipoles are calculated using Tong's model potential, which can be found in [67]. The comparison between the input and retrieved group delay $\Delta\tau_{2p/2s}$ are shown in figure 1(e) for the TL case and in figure 1(f) for the chirped case. We have retrieved this group delay using FROG-CRAB presented in [59], and now we add the result from PROBP to the comparison. The input group delay is almost constant (4–5 as). Clearly this group delay is accurately retrieved by both FROG-CRAB and PROBP if the XUV pulse has no chirp. However, in the case of chirped XUV, the retrieved group delays increase with photon energy (from −3 to 12 as for PROBP and from −10 to 20 as for FROG-CRAB). Because we actually retrieve the wave packet instead of the dipole, when the XUV phase changes rapidly but the dipole phase changes smoothly, the wave packet phase is determined by the XUV phase and becomes insensitive to the dipole phase, which lead to difficulties in extracting the latter. This problem happens in both FROG-CRAB and PROBP methods. On the other hand, we can see in figure 1(f) that the PROBP result is closer to the input than FROG-CRAB. The error is reduced by PROBP because PROBP fits the spectrograms based on WPA equation (6) without introducing CMA.

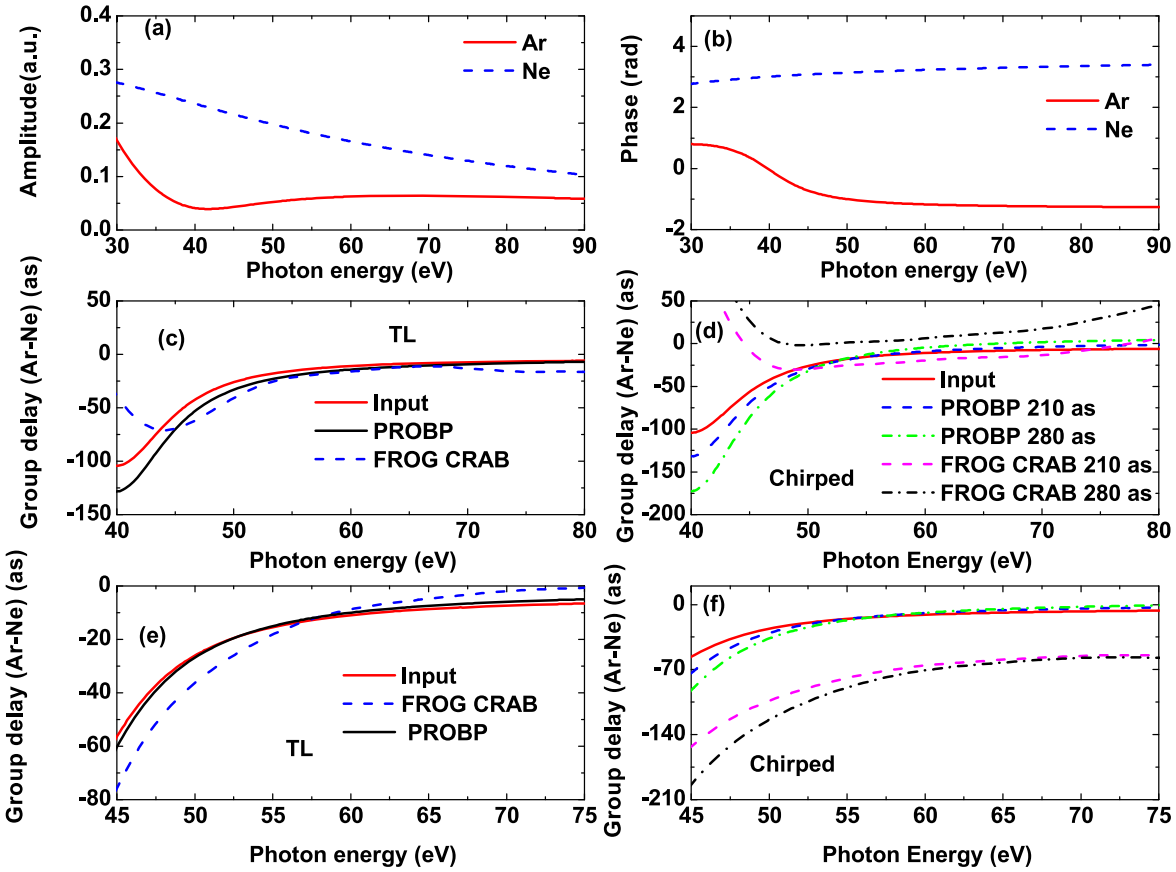

Figure 2. (a) Input dipole amplitude and (b) dipole phase for Ar and Ne targets. (c) Comparison between the input photoionization group delay (difference) $\Delta\tau_{\mathrm{Ar/Ne}}$ and the retrieved group delay from PROBP and FROG-CRAB using the 80 as TL broad-band XUV pulse. (d) Retrieved group delays from PROBP and FROG-CRAB by using two chirped XUV pulses (210 as and 280 as) whose spectral amplitude are the same as the TL pulse used in (c). (e) Comparison between the input and retrieved group delays using the 160 as TL narrow-band XUV pulse. (f) Retrieved group delays from PROBP and FROG-CRAB by using two chirped XUV pulses (210 as and 280 as) whose spectral amplitude are the same as the TL pulse used in (e), with the legend same as in (d). All XUV pulses are centered at $\Omega_0 = 60$ eV, $\Delta\Omega = 23$ eV for broad-band pulses in (c) and (d), and $\Delta\Omega = 11.5$ eV for narrow-band pulses in (e) and (f). The IR field is 800 nm in wavelength, cosine-squared envelope, 8.8 fs in FWHM duration, and 10^{12} W cm^{-2} in peak intensity.

3.2. Group delay between photoionization from Ar(3p) and Ne(2p)

In this subsection, we show the photoionization group delay (difference) $\Delta\tau_{\mathrm{Ar/Ne}}$ between Ar($3p$) and Ne($2p$) retrieved from PROBP and we compare this result with that from FROG-CRAB. The input photoionization transition dipole amplitude and phase for Ar and Ne atoms are plotted in figures 2(a) and (b), respectively. These dipoles are calculated using the model potential given in [67]. The input spectrograms are computed using equation (1). All the XUV pulses used have a central photon energy $\Omega_0 = 60$ eV, but the FWHM bandwidth are different. For narrow-band pulses, $\Delta\Omega = 11.5$ eV, supporting a TL pulse with a FWHM duration of 160 as. For broad-band pulses, $\Delta\Omega = 23$ eV, supporting a TL pulse with a duration of 80 as. The IR field is 800 nm in wavelength, cosine-squared envelope, 8.8 fs in FWHM duration, and 10^{12} W cm^{-2} in peak intensity. The input and retrieved group delays $\Delta\tau_{\mathrm{Ar/Ne}}$ are compared in figure 2(c) for the case of broad-band 80 as TL XUV pulse, and in figure 2(e) for the case of narrow-band 160 as TL XUV pulse. The FROG-CRAB results are selected from [59] in which $E_{\mathrm{shift}} = 80$ eV for the broad-band case and $E_{\mathrm{shift}} = 70$ eV for the narrow-band case. E_{shift} is the energy shift of the Ar spectrogram in order to combine the Ar and Ne spectrograms together as the input of FROG-CRAB. Details of the FROG-CRAB method have been discussed in [59]. The error of FROG-CRAB mainly comes from CMA, therefore the retrieved group delay is expected to be more accurate when using PROBP, which has been confirmed by figures 2(c) and (e). The remaining error of PROBP may come from the WPA, which will be addressed in section 4.1. From figure 2(c), we can see the error of PROBP becomes larger in the photon energy range of 40–50 eV. The input dipole phase of Ar has a big jump around 40 eV, but this energy range is outside the FWHM bandwidth of the XUV pulse (23 eV), therefore the reconstructed spectrogram is not very sensitive to the wave packet phase in this range. This can explain why it is difficult to get a good result below 50 eV.

We also test the performance of PROBP in retrieving $\Delta\tau_{\mathrm{Ar/Ne}}$ when the XUV is chirped. We have known that if the wave packet phase is dominated by the XUV phase, to extract the dipole phase is challenging. Since a certain amount of residual attochirp will always be present in a real experiment,

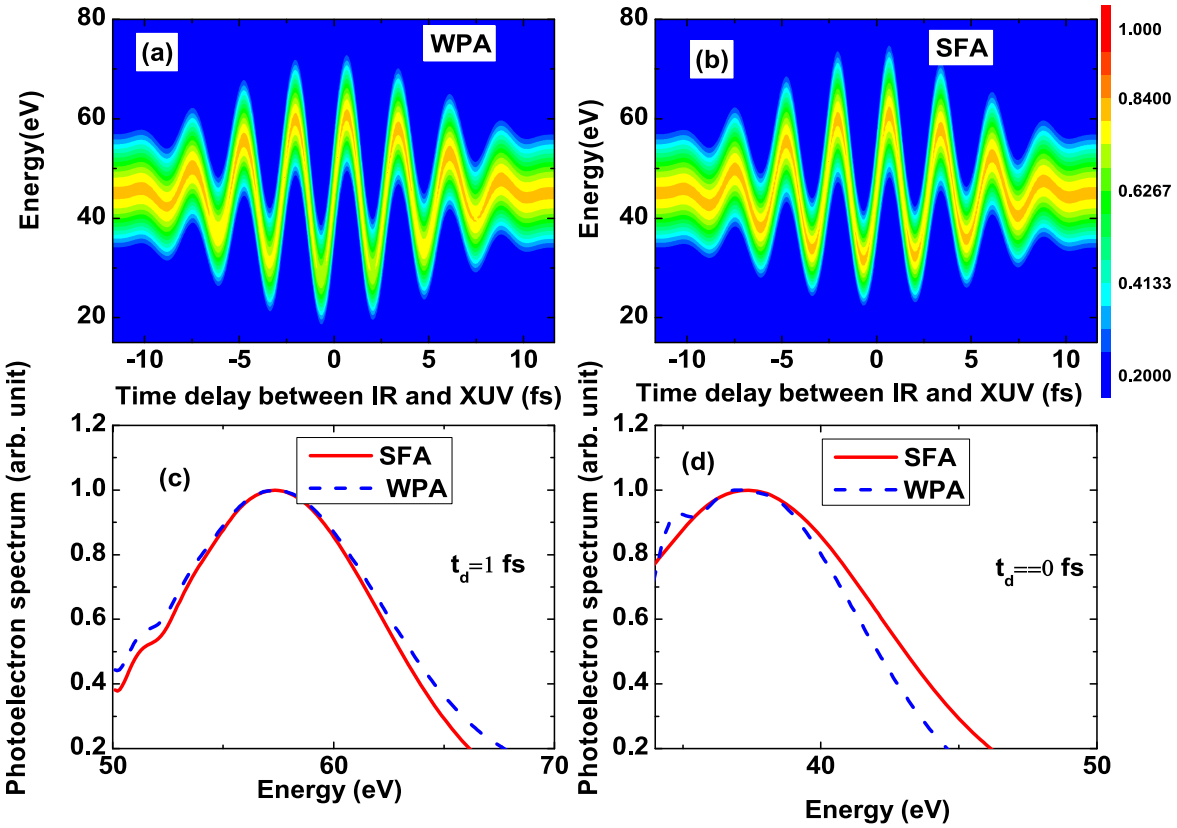

Figure 3. Spectrogram of Ar calculated (a) by WPA equation (6) (b) by SFA equation (1). (c), (d) The two line-out plots of the two 2D spectrograms at the XUV-IR delay $t_d = 1$ fs and $t_d = 0$ fs, respectively.

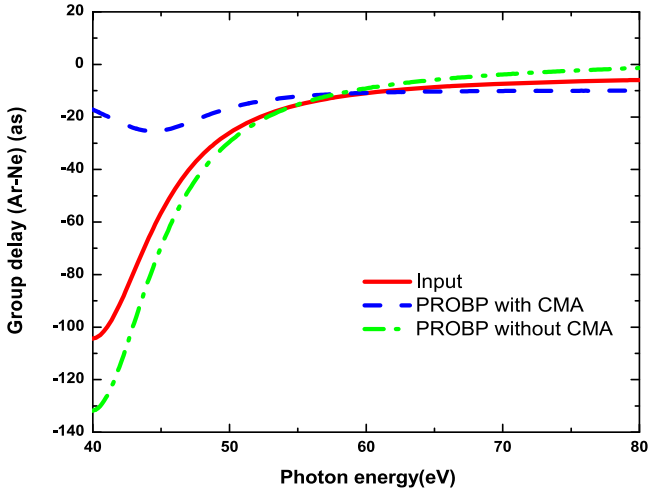

Figure 4. Comparison between the input (red solid line) photoionization group delay (difference) $\Delta\tau_{\mathrm{Ar/Ne}}$ and the retrieved group delay using PROBP including CMA (blue dashed line), and without CMA (green dot-dashed line).

the capability of PROBP to retrieve photoionization group delays with chirped XUV pulses is questioned. For the broadband case ($\Delta\Omega = 23$ eV, TL pulse duration 80 as), we use two chirped pulses with FWHM durations of 210 as ($\mathrm{GDD}_X = 0.00551$ fs^2) and 280 as ($\mathrm{GDD}_X = 0.00762$ fs^2). The retrieved group delays are shown in figure 2(d) compared with the input data. For the narrow-band case ($\Delta\Omega = 11.5$ eV, TL pulse duration 160 as), we also use two chirped pulses with FWHM durations of 210 as ($\mathrm{GDD}_X = 0.00772$ fs^2) and 280 as ($\mathrm{GDD}_X = 0.0130$ fs^2). The retrieved group delays are shown in figure 2(f). According to these figures, although the results from PROBP using chirped pulses are worse than that using TL pulses, the retrieved group delays within the XUV bandwidth are still quite acceptable. On the contrary, FROG-CRAB results for these chirped pulses are also given in figures 2(d) and (f) which illustrate much greater deviations from the input data. This is consistent with the results in [60]. We can conclude that by getting rid of the CMA, PROBP is more stable against XUV chirp than FROG-CRAB. We will address this point again in section 4.2.

4. Discussions on additional approximations beyond SFA

4.1. Accuracy of WPA used in both PROBP and FROG-CRAB

The simulations in section 3 use the SFA model equation (1) to generate input spectrograms, however the retrieval method PROBP and FROG-CRAB are based on the WPA equation (6). Since WPA is a further approximation of SFA, the inherent error of WPA may cause some error in the group delay retrieval. As an example, we calculate the streaking spectrogram for Ar using WPA equation (6), as shown in figure 3(a), and compare it with the one using equation (1)

shown in figure 3(b). The XUV pulse is the 160 as TL narrow-band ($\Delta\Omega = 11.5$ eV) pulse in section 3.2 which has been used to get figure 2(e). The IR field is 800 nm in wavelength, cosine-squared envelope, 8.8 fs in FWHM duration, and 10^{12} W cm^{-2} in peak intensity. When comparing figures 3(a) and (b), at the first glance the differences between the two 2D spectrograms are not prominent . However after plotting the photoelectron spectra at a fixed XUV-IR delay, such as $t_d = 1$ fs for figure 3(c) and $t_d = 0$ fs for figure 3(d), the difference between WPA and SFA can be observed. The error of WPA will result in the small error of PROBP shown in figure 2(e). If chirped XUV pulses are used, the WPA may also be a cause of error in retrieving the dipole phase.

4.2. Effect of CMA used in FROG-CRAB

The accuracy of FROG-CRAB is limited by the CMA. Especially when using chirped XUV pulses, the FROG-CRAB will fail to retrieve the photoionization group delay due to the breakdown of CMA [60]. Here we demonstrate the role of CMA in retrieving dipole phase by applying the B-spline fitting method including CMA. We start from the input SFA spectrograms generated by the 210 as chirped broad-band XUV pulse ($\Delta\Omega = 23$ eV, TL pulse duration 80 as) used in section 3.2. PROBP without CMA has extracted $\Delta\tau_{\mathrm{Ar/Ne}}$ from these spectrograms and the result is plotted in the green dot-dashed line in figure 4. Now we repeat the PROBP algorithm but replace $\varphi(p, t)$ in equation (6) by $\varphi(p_0, t)$ where p_0 is the central momentum, that is, we introduce CMA to PROBP. The result with CMA is shown in the blue dashed line in figure 4 compared with the input group delay in the red solid line. Clearly the retrieved group delay including CMA becomes much worse than the one without CMA. The example shows CMA is detrimental to the group delay extraction when the XUV has some kind of attochirp, which makes the FROG-CRAB less desirable. For the XUV bandwidth (11–23 eV) used in this work, [61] has demonstrated that the CMA does not cause much errors for FROG-CRAB to retrieve chirped XUV pulses. However in the sense of dipole phase retrieval, the success of FROG-CRAB cannot be guaranteed any more. When the XUV pulse is chirped, the phase of the wave packet is dominated by the large XUV phase, while the spectrogram is affected by the dipole phase only slightly. To extract such a tiny effect correctly, a more accurate model without the CMA is requested.

5. Conclusion

We have applied the PROBP method which was previously proposed to characterize broad-band attosecond pulses to the retrieval of dipole phase and therefore the photoionization group delay which is defined as the energy derivative of the dipole phase. We simulate the input streaking spectrograms for photoelectrons from (a) 2*p* and 2*s* states of Ne (b) Ar(3*p*) and Ne(2*p*) states by using SFA model. The photoionization group delay difference retrieved from PROBP has been compared with the result from FROG-CRAB. Unlike FROG-CRAB, PROBP does not rely on CMA. We have demonstrated that PROBP is in general a more accurate method than FROG-CRAB. When the XUV pulse has some attochirp, the PROBP is quite stable against XUV chirp whereas FROG-CRAB tends to fail, because the CMA becomes detrimental to the dipole phase retrieval in the case of chirped XUV. The difference between WPA and SFA has also been investigated. The error embedded in WPA will be another source of error in the group delay retrieval. Our simulation neglects the coupling effect between the photoelectron and its parent ion in the laser field. This effect is known to be insignificant for the photoelectron energy range considered in this article. To calibrate the performance of PROBP to real experimental spectrograms especially when the electron energies are not very high, *ab-initio* simulations based on solving the time-dependent Schrödinger equation may be needed in the future.

Acknowledgments

Xi Zhao, Hui Wei and C D Lin was supported in part by Chemical Sciences, Geosciences and Biosciences Division, Office of Basic Energy Sciences, Office of Science, US Department of Energy, under Grant No. DE-FG02-86ER13491. Changli Wei is supported by the introducing talent program of Qiannan Normal University for Nationalities (qnsyrc201619), People's Republic of China.

ORCID iDs

Hui Wei https://orcid.org/0000-0001-7199-4434
C D Lin https://orcid.org/0000-0003-4847-8938

References

[1] Paul P M, Toma E S, Breger P, Mullot G, Augé F, Balcou P, Muller H G and Agostini P 2001 Observation of a train of attosecond pulses from high harmonic generation *Science* **292** 1689
[2] Hentschel M, Kienberger R, Spielmann C, Reider G A, Milosevic N, Brabec T, Corkum P, Heinzmann U, Drescher M and Krausz F 2001 Attosecond metrology *Nature* **414** 509
[3] Sola I J *et al* 2006 Controlling attosecond electron dynamics by phase-stabilized polarization gating *Nat. Phys.* **2** 319
[4] Goulielmakis E *et al* 2008 Single-cycle nonlinear optics *Science* **320** 1614
[5] Jullien A, Pfeifer T, Abel M J, Nagel P M, Bell M J, Neumark D M and Leone S R 2008 Ionization phase-match gating for wavelength-tunable isolated attosecond pulse generation *Appl. Phys.* B **93** 433
[6] Mashiko H, Gilbertson S, Li C, Khan S D, Shakya M M, Moon E and Chang Z 2008 Double optical gating of high-order harmonic generation with carrier-envelope phase stabilized lasers *Phys. Rev. Lett.* **100** 103906
[7] Zhao K, Zhang Q, Chini M, Wu Y, Wang X and Chang Z 2012 Tailoring a 67 attosecond pulse through advantageous phase-mismatch *Opt. Lett.* **37** 3891

[8] Kim K T, Zhang C, Ruchon T, Hergott J F, Auguste T, Villeneuve D M, Corkum P B and Quéré F 2013 Photonic streaking of attosecond pulse trains *Nat. Photon.* **7** 651

[9] Ishii N, Kaneshima K, Kitano K, Kanai T, Watanabe S and Itatani J 2014 Carrier-envelope phase-dependent high harmonic generation in the water window using few-cycle infrared pulses *Nat. Commun.* **5** 3331

[10] Cousin S L, Silva F, Teichmann S, Hemmer M, Buades B and Biegert J 2014 High-flux table-top soft x-ray source driven by sub-2-cycle, CEP stable, 1.85 mm 1 kHz pulses for carbon K-edge spectroscopy *Opt. Lett.* **39** 5383

[11] Ding C, Xiong W, Fan T, Hickstein D D, Popmintchev T, Zhang X, Walls M, Murnane M M and Kapteyn H C 2014 High flux coherent super-continuum soft x-ray source driven by a single-stage, 10 mJ, Ti:sapphire amplifier-pumped OPA *Opt. Express* **22** 6194

[12] Silva F, Teichmann S M, Cousin S L, Hemmer M and Biegert J 2015 Spatiotemporal isolation of attosecond soft x-ray pulses in the water window *Nat. Commun.* **6** 6611

[13] Li J, Ren X, Yin Y, Cheng Y, Cunningham E, Wu Y and Chang Z 2016 Polarization gating of high harmonic generation in the water window *Appl. Phys. Lett.* **108** 231102

[14] Drescher M, Hentschel M, Kienberger R, Uiberacker M, Yakovlev V, Scrinzi A, Westerwalbesloh T, Kleineberg U, Heinzmann U and Krausz F 2002 Time-resolved atomic inner-shell spectroscopy *Nature* **419** 803

[15] Swoboda M, Fordell T, Klünder K, Dahlström J M, Miranda M, Buth C, Schafer K J, Mauritsson J, L'Huillier A and Gisselbrecht M 2010 Phase measurement of resonant two-photon ionization in helium *Phys. Rev. Lett.* **104** 103003

[16] Klünder K *et al* 2011 Probing single-photon ionization on the attosecond time scale *Phys. Rev. Lett.* **106** 143002

[17] Guénot D *et al* 2012 Photoemission-time-delay measurements and calculations close to the 3s-ionization-cross-section minimum in Ar *Phys. Rev.* A **85** 053424

[18] Guénot D *et al* 2014 Measurements of relative photoemission time delays in noble gas atoms *J. Phys. B: At. Mol. Opt. Phys.* **47** 245602

[19] Palatchi C, Dahlström J M, Kheifets A S, Ivanov I A, Canaday D M, Agostini P and DiMauro L F 2014 Atomic delay in helium, neon, argon and krypton *J. Phys. B: At. Mol. Opt. Phys.* **47** 245003

[20] Heuser S *et al* 2016 Angular dependence of photoemission time delay in helium *Phys. Rev.* A **94** 063409

[21] Gruson V *et al* 2016 Attosecond dynamics through a Fano resonance: monitoring the birth of a photoelectron *Science* **354** 734

[22] Schultze M *et al* 2010 Delay in photoemission *Science* **238** 1658

[23] Sabbar M, Heuser S, Boge R, Lucchini M, Carette T, Lindroth E, Gallmann L, Cirelli C and Keller U 2015 Resonance effects in photoemission time delays *Phys. Rev. Lett.* **115** 133001

[24] Ossiander M *et al* 2017 Attosecond correlation dynamics *Nat. Phys.* **13** 280

[25] Uiberacker M *et al* 2007 Attosecond real-time observation of electron tunnelling in atoms *Nature* **446** 627

[26] Eckle P, Pfeiffer A N, Cirelli C, Staudte A, Dörner R, Muller H G, Büttiker M and Keller U 2008 Attosecond ionization and tunneling delay time measurements in helium *Science* **322** 1525

[27] Tzallas P, Skantzakis E, Nikolopoulos L A A, Tsakiris G D and Charalambidis D 2011 Extreme-ultraviolet pump-probe studies of one-femtosecond-scale electron dynamics *Nat. Phys.* **7** 781

[28] Landsman A S, Weger M, Maurer J, Boge R, Ludwig A, Heuser S, Cirelli C, Gallmann L and Keller U 2014 Ultrafast resolution of tunneling delay time *Optica* **1** 343

[29] Månsson E P *et al* 2014 Double ionization probed on the attosecond timescale *Nat. Phys.* **10** 207

[30] Caillat J, Maquet A, Haessler S, Fabre B, Ruchon T, Salières P, Mairesse Y and Taïeb R 2011 Attosecond resolved electron release in two-color near-threshold photoionization of N_2 *Phys. Rev. Lett.* **106** 093002

[31] Kelkensberg F *et al* 2011 Attosecond control in photoionization of hydrogen molecules *Phys. Rev. Lett.* **107** 043002

[32] Sansone G *et al* 2010 Electron localization following attosecond molecular photoionization *Nature* **465** 763

[33] Calegari F *et al* 2014 Ultrafast electron dynamics in phenylalanine initiated by attosecond pulses *Science* **346** 336

[34] Trabattoni A *et al* 2015 Mapping the dissociative ionization dynamics of molecular nitrogen with attosecond time resolution *Phys. Rev.* X **5** 041053

[35] Cavalieri A L *et al* 2007 Attosecond spectroscopy in condensed matter *Nature* **449** 1029

[36] Neppl S, Ernstorfer R, Bothschafter E M, Cavalieri A L, Menzel D, Barth J V, Krausz F, Kienberger R and Feulner P 2012 Attosecond time-resolved photoemission from core and valence states of magnesium *Phys. Rev. Lett.* **109** 087401

[37] Neppl S *et al* 2015 Direct observation of electron propagation and dielectric screening on the atomic length scale *Nature* **517** 342

[38] Lemell C, Neppl S, Wachter G, Tőkési K, Ernstorfer R, Feulner P, Kienberger R and Burgdörfer J 2015 Real-time observation of collective excitations in photoemission *Phys. Rev.* B **91** 241101

[39] Locher R, Castiglioni L, Lucchini M, Greif M, Gallmann L, Osterwalder J, Hengsberger M and Keller U 2015 Energy-dependent photoemission delays from noble metal surfaces by attosecond interferometry *Optica* **2** 405

[40] Tao Z, Chen C, Szilvási T, Keller M, Mavrikakis M, Kapteyn H and Murnane M 2016 Direct time-domain observation of attosecond final-state lifetimes in photoemission from solids *Science* **353** 62

[41] Itatani J, Quéré F, Yudin G L, Ivanov M Y, Krausz F and Corkum P B 2012 Attosecond streak camera *Phys. Rev. Lett.* **88** 173903

[42] Muller H G 2002 Reconstruction of attosecond harmonic beating by interference of two-photon transitions *Appl. Phys.* B **74** S17

[43] Mairesse Y and Quéré F 2005 Frequency-resolved optical gating for complete reconstruction of attosecond bursts *Phys. Rev.* A **71** 011401

[44] Eisenbud L 1948 Formal properties of nuclear collisions *PhD Thesis* Princeton University

[45] Wigner E P 1955 Lower limit for the energy derivative of the scattering phase shift *Phys. Rev.* **98** 145

[46] Smith F T 1960 Lifetime matrix in collision theory *Phys. Rev.* **118** 349

[47] Maquet A, Caillat J and Taïeb R 2014 Attosecond delays in photoionization: time and quantum mechanics *J. Phys. B: At. Mol. Opt. Phys.* **47** 204004

[48] Pazourek R, Nagele S and Burgdörfer J 2015 Attosecond chronoscopy of photoemission *Rev. Mod. Phys.* **87** 765

[49] Ivanov M and Smirnova O 2011 How accurate is the attosecond streak camera? *Phys. Rev. Lett.* **107** 213605

[50] Zhang C H and Thumm U 2010 Electron-ion interaction effects in attosecond time-resolved photoelectron spectra *Phys. Rev.* A **82** 043405

[51] Su J, Ni H, Becker A and Jaron-Becker A 2013 Numerical simulation of time delays in light-induced ionization *Phys. Rev.* A **87** 033420
[52] Su J, Ni H, Becker A and Jaron-Becker A 2013 Finite-range time delays in numerical attosecond-streaking experiments *Phys. Rev.* A **88** 023413
[53] Nagele S, Pazourek R, Feist J and Burgdörfer J 2012 Time shifts in photoemission from a fully correlated two-electron model system *Phys. Rev.* A **85** 033401
[54] Pazourek R, Feist J, Nagele S and Burgdörfer J 2012 Attosecond streaking of correlated two-electron transitions in helium *Phys. Rev. Lett.* **108** 163001
[55] Kheifets A S and Ivanov I A 2010 Delay in atomic photoionization *Phys. Rev. Lett.* **105** 233002
[56] Moore L R, Lysaght M A, Parker J S, van der Hart H W and Taylor K T 2011 Time delay between photoemission from the 2*p* and 2*s* subshells of neon *Phys. Rev.* A **84** 061404
[57] Dahlström J M, Carette T and Lindroth E 2012 Diagrammatic approach to attosecond delays in photoionization *Phys. Rev.* A **86** 061402(R)
[58] Feist J, Zatsarinny O, Nagele S, Pazourek R, Burgdörfer J, Guan X, Bartschat K and Schneider B I 2014 Time delays for attosecond streaking in photoionization of neon *Phys. Rev.* A **89** 033417
[59] Wei H, Morishita T and Lin C D 2016 Critical evaluation of attosecond time delays retrieved from photoelectron streaking measurements *Phys. Rev.* A **93** 053412
[60] Cattaneo L, Vos J, Lucchini M, Gallmann L, Cirelli C and Keller U 2016 Comparison of attosecond streaking and RABBITT *Opt. Express* **24** 029066
[61] Zhao X, Wei H, Wu Y and Lin C D 2017 Phase-retrieval algorithm for the characterization of broadband single attosecond pulses *Phys. Rev.* A **95** 043407
[62] Kitzler M, Milosevic N, Scrinzi A, Krausz F and Brabec T 2002 Quantum theory of attosecond XUV pulse measurement by laser dressed photoionization *Phys. Rev. Lett.* **88** 173904
[63] Yakovlev V S, Gagnon J, Karpowicz N and Krausz F 2010 Attosecond streaking enables the measurement of quantum phase *Phys. Rev. Lett.* **105** 073001
[64] Kane D 1999 Recent progress toward real-time measurement of ultrashort laser pulses *IEEE J. Quantum Electron.* **35** 421
[65] Gagnon J, Goulielmakis E and Yakovlev V S 2008 The accurate FROG characterization of attosecond pulses from streaking measurements *Appl. Phys.* B **92** 25
[66] Bachau H, Cormier E, Decleva P, Hansen J E and Martín F 2001 Applications of B-splines in atomic and molecular physics *Rep. Prog. Phys.* **64** 1815
[67] Tong X M and Lin C D 2005 Empirical formula for static field ionization rates of atoms and molecules by lasers in the barrier-suppression regime *J. Phys. B: At. Mol. Opt. Phys.* **38** 2593